

Thermal induced structural and magnetic transformations in $\text{Fe}_{73.5-x}\text{Ce}_{x=0,3,5,7}\text{Si}_{13.5}\text{B}_9\text{Nb}_3\text{Cu}_1$ amorphous alloy

Małgorzata Antoszewska · Michał Wasiak ·
Tomasz Gwizdała · Pavol Sovak · Marek Moneta

Received: 17 July 2013 / Accepted: 6 September 2013 / Published online: 22 October 2013
© The Author(s) 2013. This article is published with open access at Springerlink.com

Abstract Structural and magnetic properties of amorphous and partly crystallized $\text{Fe}_{73.5-x}\text{Ce}_{x=0,3,5,7}\text{Si}_{13.5}\text{B}_9\text{Nb}_3\text{Cu}_1$ alloys, were analysed in the temperature ranging from RT to 800 °C with scanning calorimetry and magnetometry. The Fe(Si) and Fe(B) structures were identified and characterised with set of crystallization temperatures and activation energies. Also, Curie temperatures for amorphous and for crystalline structures were determined and analysed as functions of Ce content.

Keywords Amorphous alloys · Ce compounds · Scanning calorimetry · Thermomagnetometry

Introduction

Alloys, like $\text{Fe}_{73.5}\text{Cu}_1\text{Si}_{13.5}\text{B}_9\text{Nb}_3$ classical finemet, appear primarily in amorphous-magnetic phase, which after appropriate thermal or mechanical treatment, are transformed into the phase, when iron-silicides and -borides magnetic nano-crystals are embedded in an amorphous residual matrix [1–3]. For practical purpose, in order to obtain soft magnetic properties of the material, it is

important that the size of nano-crystals, during primary crystallization, is smaller than the exchange correlation length.

So far, many different modifications of the basic FeSiB composition were analysed while searching for better technical properties [4–10]. The analysis was focused rather on products of primary crystallization at lower annealing temperatures with less interest on the secondary crystallization.

In this work mainly secondary crystallization at higher temperatures and its correlation to magnetization phenomena of $\text{Fe}_{73.5-x}\text{Ce}_{x=0,3,5,7}\text{Si}_{13.5}\text{B}_9\text{Nb}_3\text{Cu}_1$, (a finemet with Ce substituted for Fe), was analysed by means of scanning calorimetry (DSC) and, performed at the same time, thermomagnetic measurements (TM). Identification of structures and magnetic properties of the present alloys, was based on our previous DSC, XRD and Mössbauer spectroscopy study [7, 8] of the alloys with dopants other than Ce.

Samples were prepared by casting melt on a rapidly rotating copper wheel, thus cooling it at 10^7 K s^{-1} and solidifying in the form of 20- μm thick bands of amorphous alloy.

Results and discussion

Differential scanning calorimetry DSC

The scans of DSC heat flow as function of temperature were performed on Setaram DSC 111 at heating rates ranging from 1 to 20 K min^{-1} with samples of various ($\sim 10 \text{ mg}$) masses in the ambient N_2 environment. All scans in Figs. 1 and 2 display in fact two main structures, identified in the previous studies [7, 8], of the same basic

M. Antoszewska (✉) · T. Gwizdała · M. Moneta
Wydział Fizyki i Informatyki Stosowanej, Uniwersytet Łódzki,
Pomorska 149, 90-236 Lodz, Poland
e-mail: m_ateno@interia.pl

M. Wasiak
Wydział Chemii, Katedra Chemii Fizycznej, Uniwersytet
Łódzki, Pomorska 165, 90-236 Lodz, Poland

P. Sovak
Department of Condensed Matter Physics, P.J. Šafárik
University Košice, Park Angelinum 9, 041-54 Kosice, Slovakia

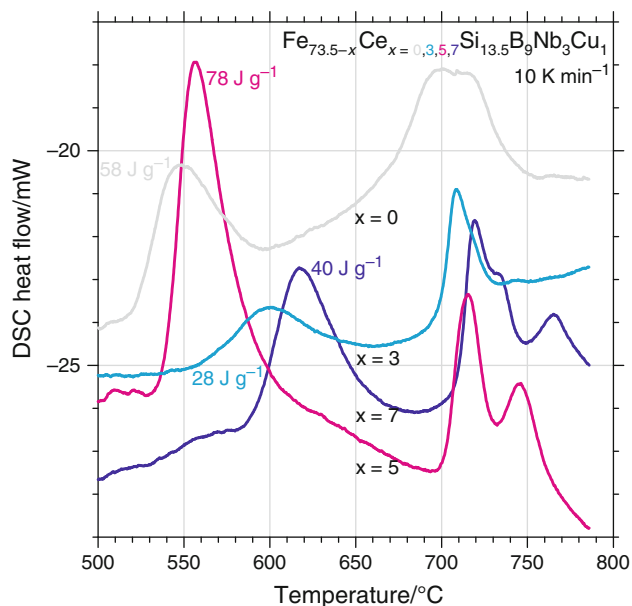


Fig. 1 $\text{Fe}_{73.5-x}\text{Ce}_{x=0,3,5,7}\text{Si}_{13.5}\text{B}_9\text{Nb}_3\text{Cu}_1$ alloys: DSC scans of at heating rate 10 K min^{-1} . Localization of peaks, temperatures of maxima and specific enthalpies for primary (peak 1) and secondary (peaks 2 and 3) crystallization, in dependence on Ce content $x = 0, 3, 5, 7$

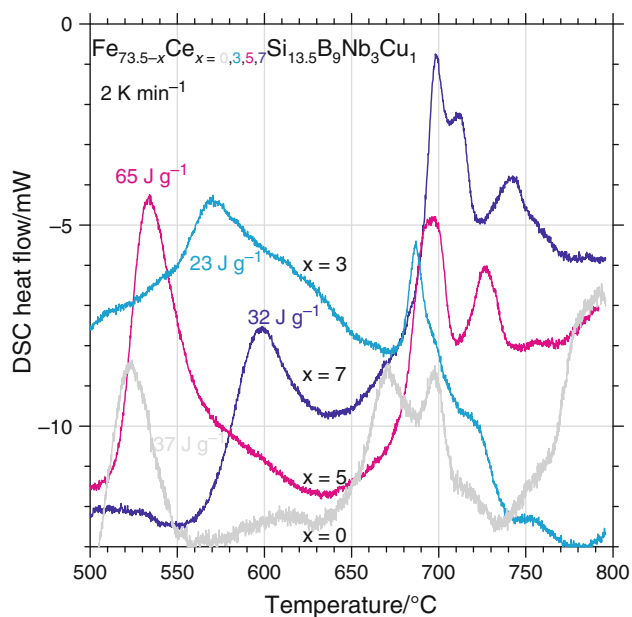


Fig. 2 As in Fig. 1, but at heating rate 2 K min^{-1}

alloy but with other dopants. The first peak corresponds to primary crystallization of silicides, mainly Fe_3Si with onset points at $450\text{--}480\text{ }^\circ\text{C}$ [2, 7]. The secondary structure is related to crystallization of borides, mainly Fe_3B and Fe_{23}B_6 . Fe_3B crystallizes at $540\text{--}600\text{ }^\circ\text{C}$ [2, 7], whereas Fe_{23}B_6 precipitates at $400\text{ }^\circ\text{C}$ and at $670\text{--}740\text{ }^\circ\text{C}$ [9]. Phase transfer parameters substantially depend on composition of

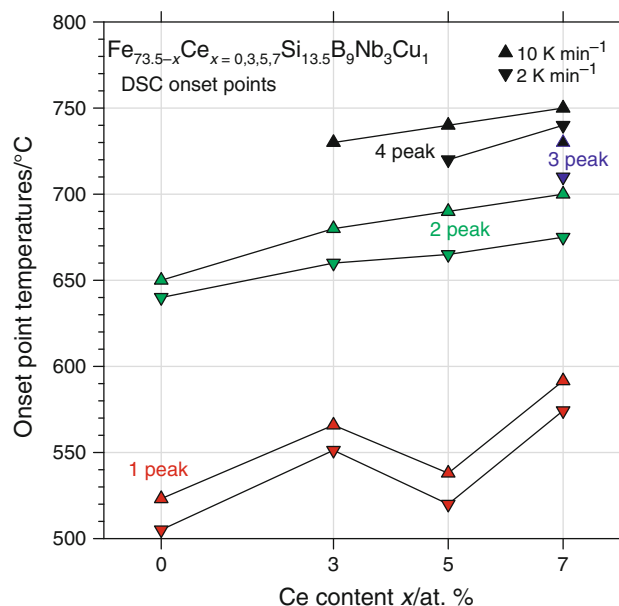


Fig. 3 Crystallization onset points from DSC scans of $\text{Fe}_{73.5-x}\text{Ce}_{x=0,3,5,7}\text{Si}_{13.5}\text{B}_9\text{Nb}_3\text{Cu}_1$ alloys at heating rate 2 K min^{-1} (inverted triangle) and 10 K min^{-1} (triangle)

the alloy and on details of thermal treatment. Crystallographic structures, expected to appear, were previously disclosed and analysed in detail with XRD and Mössbauer spectroscopy by using alloys which were annealed for 1 h at temperatures specified by DSC [7, 8].

In Figs. 1 and 2, primary crystallization starts at the onset point of approximately $500\text{--}550\text{ }^\circ\text{C}$, which strongly depends on the Ce content. The peaks are well resolved and allow us to calculate crystallization enthalpies and activation energies, along evolutionary procedure [11]. Secondary crystallization starts at about $650\text{ }^\circ\text{C}$, and addition of Ce reveals that it is represented by double peaks for Ce_3 and Ce_5 or even by triple peaks for Ce_7 , which suggests complicated structure of the alloy with higher Ce content. An overall increase of the onset temperature for the selected peaks with the Ce content x and heating rate is presented in Fig. 3. There is, however, some exception to primary crystallization onset temperature for the alloy with Ce_5 . It can be expected that the structure, which is disclosed during secondary crystallization of the present alloy, would be more complicated for $x > 7$.

The effective activation energy for crystallization E_a can be determined from the Kissinger equation:

$$\frac{v}{T_p^2} = A \times \exp \frac{-E_a}{R \times T_p}, \quad (1)$$

where v is the temperature increase rate, $R = 8.31\text{ J mol}^{-1}\text{ K}^{-1}$ is the gas constant, T_p is the peak temperature and A is a constant. The activation energies E_a were calculated by fitting data points with Eq. (1). The

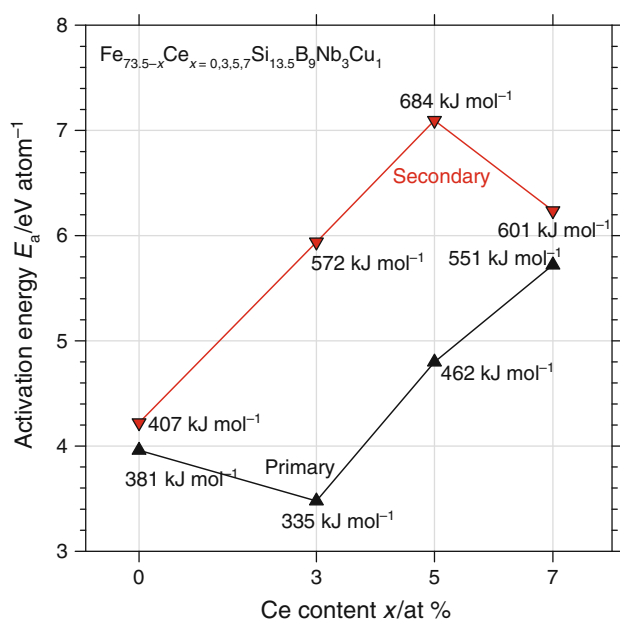


Fig. 4 $\text{Fe}_{73.5-x}\text{Ce}_{x=0,3,5,7}\text{Si}_{13.5}\text{B}_9\text{Nb}_3\text{Cu}_1$: activation energies E_a for primary (peak 1, triangle) and secondary (peaks 2 and 3, inverted triangle) crystallization shown in Figs. 1 and 2, in dependence on Ce content x , calculated from the Kissinger equation, Eq. (1)

calculated activation energy for primary crystallization of pure finemet ($x = 0$) $E_a = 381 \text{ kJ mol}^{-1}$ closely corresponds to the value of 384 kJ mol^{-1} found in Ref. [2]. The E_a values for other x , namely for Ce_3 , Ce_5 and Ce_7 , are presented in Fig. 4. As it is seen in the figure, E_a slightly increases with Ce content x from 381 to 551 kJ mol^{-1} for primary crystallization and from 401 to 684 kJ mol^{-1} for secondary crystallization. This would suggest either structure with empty nano-regions requiring energy consuming rearrangement or an initial thermal treatment (or aging) of the amorphous alloy followed by precipitation of some Fe(Si) nanocrystals and enrichment of the residual amorphous phase with Nb and B, which makes further crystallization more difficult.

Enthalpy H_x^0 gained for phase formations depend on heating speed v and on Ce content $x = 0, 3, 5, 7$. For primary peak, corresponding to formation of silicides, H_x^0 's are shown in Table 1. There is no clear dependence of the parameters on Ce contents; it seems that the material with $x = 7$ reveals decreased the values than should be expected. The determined values should be compared with the latent heat for Fe of 12.7 kJ mol^{-1} .

Thermomagnetometry TM

The thermomagnetic (TM) measurement of material magnetization was performed with Setaram-111 in TG-DSC mode. A small neodymium magnet used to produce a magnetic field $B \approx 0.75 \text{ mT}$ around the sample and a

Table 1 Phase formation enthalpy $H_x^0/\text{kJ mol}^{-1}$ for primary peak in $\text{Fe}_{73.5-x}\text{Ce}_{x=0,3,5,7}\text{Si}_{13.5}\text{B}_9\text{Nb}_3\text{Cu}_1$ alloys, shown in Figs. 1 and 2, as functions of Ce content x and of the temperature increase rate $v/\text{K min}^{-1}$

v	$x = 0$	$x = 3$	$x = 5$	$x = 7$
2	1.896	1.263	3.612	1.878
10	3.012	1.540	4.355	2.267

magnetic field gradient $-\nabla B \approx 0.14 \text{ mT cm}^{-1}$ parallel to the sample surface. This set-up was used rather as an indicator, than as a tool for precise measurement of the sample magnetization. The measurements were performed on $\sim 12 \text{ mg}$ mass samples placed in the N_2 ambient atmosphere at various heating rates. The temperature ranged from RT up to 1073 K (and backwards).

Examples of the scans for Ce content from $x = 3$ to $x = 7$, which were heated at 10 and 2 K min^{-1} , are shown in Figs. 5 and 6, where magnetization M was measured via mass change dm . Initially, during the primary increase of temperature (TM 1up), M displays one abrupt fall to zero value. During the next three runs: when temperature decreases (TM 1down), then increases again (TM 2up) and finally decreases (TM 2down), the M scans run along nearly the same curve, which reveals at least three characteristic regions. The magnetization scans were numerically deconvoluted with evolutionary algorithm [11], by fitting Brillouin functions in these regions. M was measured simultaneously with the corresponding DSC scan, which is shown in the figures with thick-black line. Physically, each alloy is initially amorphous and ferromagnetic and it remains amorphous up to the primary crystallization onset point reported in Fig. 3, at approximately $550 \text{ }^\circ\text{C}$. The primarily amorphous phase losses ferromagnetic properties at the Curie temperature, approximately at $300 \text{ }^\circ\text{C}$, as is presented in Fig. 7. At this temperature total magnetization of the sample drops by approximately $\delta M \approx 7\text{--}10 \text{ Am}^2 \text{ kg}^{-1}$, as it is shown in Figs. 5 and 6 with thick line (TM 1up). Pursuing further along TM curve there is no magnetic response from the amorphous nonmagnetic sample when crystalline structures are formed in correlation with exo-energetic peaks on DSC scans in the figures. This means that the Curie temperatures are situated below crystallization onset points for the phases.

When sample undergoes further cooling–heating–cooling cycle, magnetization in Figs. 5 and 6 follows along TM 1down, TM 2up and TM 2down closely running curves, respectively. Each curve can be generally decomposed into three Brillouin functions related to magnetic response of structures created during primary heating. Two most noticeable Brillouin functions give the Curie temperatures $380\text{--}400$ and $630\text{--}650 \text{ }^\circ\text{C}$, but there is also a small

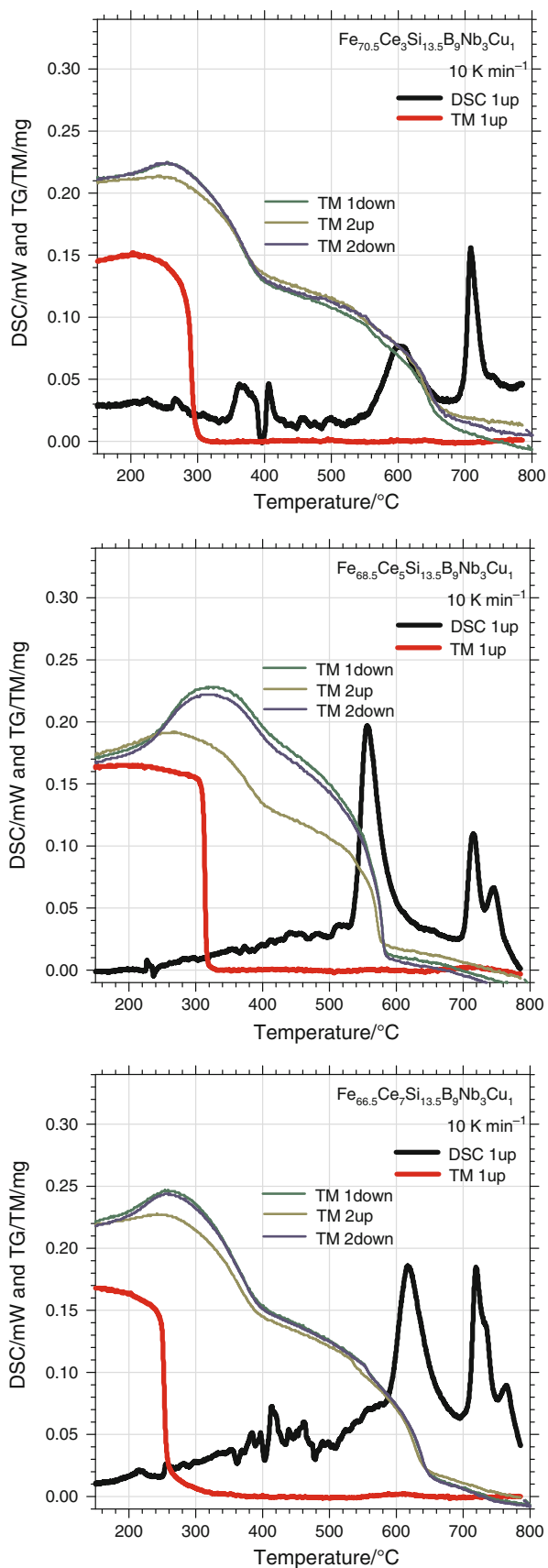


Fig. 5 $\text{Fe}_{73.5-x}\text{Ce}_x\text{Si}_{13.5}\text{B}_9\text{Nb}_3\text{Cu}_1$ alloys. TM temperature scans at 10 K min^{-1} , for $x = 3, 5, 7$ from top to bottom, respectively. TM scan during first heating of initial sample is shown with (1up). The similarly running three curves represent subsequent TM scans for: first cooling (1down), second heating (2up) and second cooling (2down). DSC reference scan taken simultaneously during first heating is shown (1up), Figs. 1 and 2. The sample mass change $dm \sim 20 \mu\text{g}$ corresponds to change of magnetization $dM \sim 1 \text{ A m}^2 \text{ kg}^{-1}$

component in the alloy, which responds magnetically at $550 \text{ }^\circ\text{C}$. They correspond to nanocrystalline Fe(Si) and Fe(B) phases, with some admixture of Ce, which precipitated from amorphous structure during primary heating.

From previous study of Finemet subjected to annealing we can expect precipitation of Fe_3Si , Fe_3B and Fe_{23}B_6 nano-structures with some additional contribution of solid solutions. Ferromagnetic bcc-Fe(Si) crystallizes at $510 \text{ }^\circ\text{C}$ and its Curie temperature is $570 \text{ }^\circ\text{C}$. Primary crystallization of fcc- Fe_{23}B_6 takes place at $400 \text{ }^\circ\text{C}$ and the secondary at $670\text{--}740 \text{ }^\circ\text{C}$ [9], whereas the Curie temperature for the phase is $420 \text{ }^\circ\text{C}$. Crystallization of t- Fe_3B is reported at $540\text{--}600 \text{ }^\circ\text{C}$ [2, 7], whereas the Curie temperature is about $520 \text{ }^\circ\text{C}$ [7, 9]. Phase transformation parameters depend on environment where the structure is embedded. In the present case Curie temperatures for the separated phase, determined as functions of Ce content x , are shown in Fig. 7, where weak dependence of T_C on x is, due to an unknown reason, slightly disturbed at C_5 .

Magnetization of amorphous phase increases nearly linearly from 5 to $10 \text{ A m}^2 \text{ kg}^{-1}$, as the Ce content x changes from 0 to 7 (also with some exception to C_5), as it is shown in Fig. 7 with numbers in mass units μg^{-1} . Also, magnetization related to first Brillouin function increases significantly from 0.5 to $5 \text{ A m}^2 \text{ kg}^{-1}$, as the Ce content x changes from 0 to 7. For the last Brillouin function magnetization changes irregularly from 1.3 to $3 \text{ A m}^2 \text{ kg}^{-1}$ reaching higher values for $x = 3$ and 5 . The remaining magnetization of the sample at RT is approximately twice as high as the initial magnetization $\sim 8\text{--}15 \text{ A m}^2 \text{ kg}^{-1}$.

Since amorphous ferromagnets, similarly to crystalline ones, reveal spin wave excitations, the low temperature magnetization $M(T)$ can be fitted with the Bloch equation:

$$\frac{\Delta M}{M(0)} = B \times T^{3/2} + C \times T^{5/2} \quad (2)$$

where $\Delta M = M(0) - M(T)$ and the B and C parameters of the order $10^{-5} \text{ K}^{-3/2}$ and $10^{-8} \text{ K}^{-5/2}$, respectively were found by fitting experimental data of Figs. 5 and 6 with Eq. (2). Calculation of B and C allows us to determine the spin-wave stiffness constants $D \approx 10^2 \text{ meV } \text{\AA}^2$ and find the mean square ranges of exchange interaction $\langle r^2 \rangle \approx 10 \text{ } \text{\AA}^2$, considerably less than for crystalline ferromagnets.

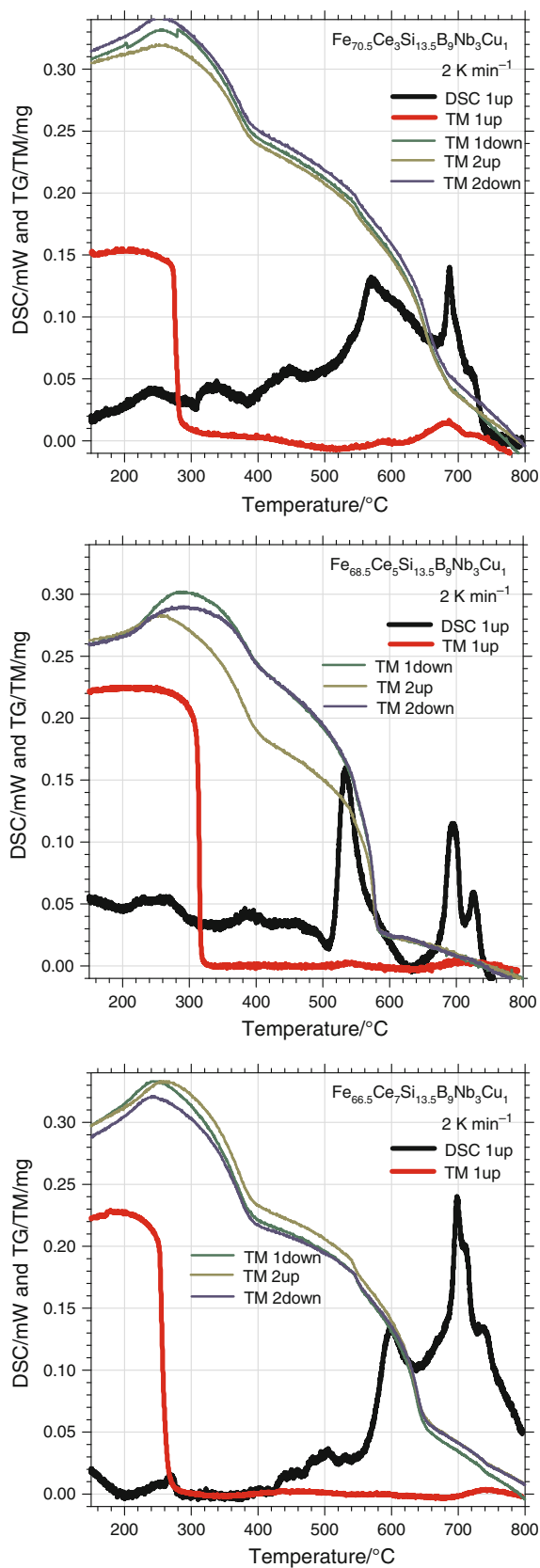


Fig. 6 As in Fig. 5, but at 2 K min^{-1}

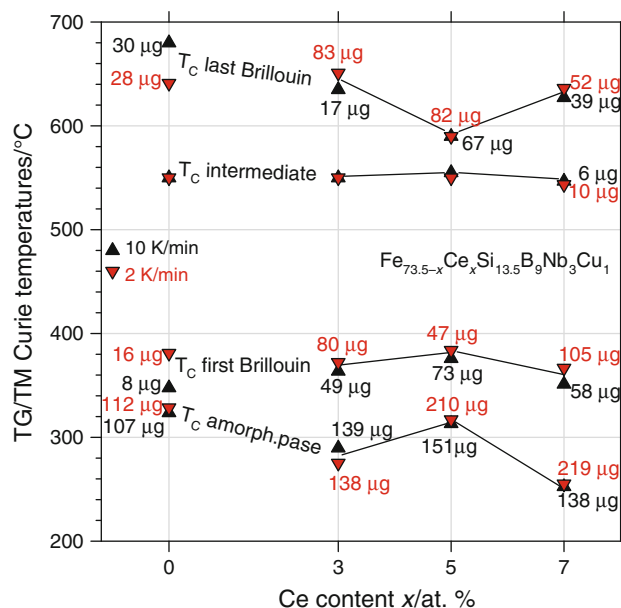


Fig. 7 $\text{Fe}_{73.5-x}\text{Ce}_x\text{Si}_{13.5}\text{B}_9\text{Nb}_3\text{Cu}_1$ alloys: Curie temperatures T_C for amorphous phase and for successive crystalline phases, in dependence on Ce content, as they appear in Figs. 5 and 6). T_C were obtained from fitting Brillouin functions to TG/TM scans measured at temperature increase rates 2 K min^{-1} (inverted triangle) and 10 K min^{-1} (triangle). Numbers refer to magnitude of magnetization change dM at T_C specified via variation of the sample mass dm : $dm \sim 20 \mu\text{g}$ corresponds to $dM \sim 1 \text{ A m}^2 \text{ kg}^{-1}$

It implies a range of exchange interaction extending up to fourth or fifth nearest neighbours.

Also, it can be shown that close to the Curie temperature for amorphous phase $\approx 300 \text{ }^{\circ}\text{C}$, the experimental data is better approximated by the Heisenberg model with critical exponent $\alpha = 0.325$, than by the Weiss mean field model with $\alpha = 0.5$. This can be understood in terms of taking statistical average in the Heisenberg hamiltonian H : in the Heisenberg model the spin correlations are taken into account and H contains terms $\langle s_i s_j \rangle$, whereas in the mean field model the correlations are disregarded and H contains forms $\langle s_i \rangle$, $\langle s_j \rangle$, where s_i , s_j are spins of the lattice sites i , j .

Conclusions

Properties of thin $\text{Fe}_{73.5-x}\text{Ce}_x\text{Si}_{13.5}\text{B}_9\text{Nb}_3\text{Cu}_1$ alloy were measured and analysed with complementary methods DSC and TM. The Curie temperature for amorphous phase reaches $320 \text{ }^{\circ}\text{C}$ and drops to $250 \text{ }^{\circ}\text{C}$ for alloys with C_3 , C_7 , respectively. Although the alloys crystallise in principle in two steps, the secondary crystallization reveals at least three tiny phases, which become separated at higher Ce content. The crystalline phases in the alloys exhibit four Curie temperatures which are rather independent on Ce

content. Also, magnitude of magnetic properties do not dramatically change with Ce.

Open Access This article is distributed under the terms of the Creative Commons Attribution License which permits any use, distribution, and reproduction in any medium, provided the original author(s) and the source are credited.

References

1. Herzer G. Grain size dependence of coercivity and permeability in nanocrystalline ferromagnets. *IEEE Trans Magn.* 1990;26:1397.
2. Chen WZ, Ryder PL. X-ray and differential scanning calorimetry study of the crystallization of amorphous $\text{Fe}_{73.5}\text{Cu}_1\text{Si}_{13.5}\text{B}_9\text{Nb}_3$ alloy. *Mater Sci Eng B.* 1995;B34:204.
3. Okumura H, Laughlin DE, McHenry ME. Magnetic and structural properties and crystallization behavior of Si-rich finemet materials. *J Magn Magn Mater.* 2003;267:347–356.
4. Czepe T. Mechanism and kinetics of nano-crystallization of the thermally stable $\text{NiNb}(\text{ZrTi})\text{Al}$ metallic glasses. *J Therm Anal Calorim.* 2010;101:615–622.
5. Ch X, Lu H, Li Y. Kinetics of non-isothermal crystallization in $\text{Cu}_{50}\text{Zr}_{43}\text{Al}_7$ and $(\text{Cu}_{50}\text{Zr}_{43}\text{Al}_7)_{95}\text{B}_5$. *J Therm Anal Calorim.* 2013. doi:10.1007/s10973-013-3364-0.
6. Kulik T, Ferenc J, Kolano-Burian A, Liang XB, Kowalczyk M. Magnetically soft nanomaterials for high-temperature applications. *J Alloys Compd.* 2007;434:623–627.
7. Brzozowski R, Wasiak M, Piekarski H, Sovak P, Uznański P, Moneta M. Properties of Mn doped finemet. *J Alloys Compd.* 2009;470:5.
8. Brzozowski R, Moneta M. Correlation between thermal induced structural and magnetic transformations in Si-rich $\text{Fe}_{73}\text{Cu}_{1-x}\text{Si}_{16}\text{B}_7\text{Nb}_3$ metal alloy. *Nucl Instrum Method Phys Res B.* 2012; B279:208.
9. Long J, Ohodnicki PR, Laughlin DE, McHenry ME, Ohkubo T, Hono K. Structural studies of secondary crystallization products of the Fe_{23}B_6 -type in a nanocrystalline FeCoB-based alloy. *J Appl Phys.* 2007;101:09N114.
10. Ponpandian N, Narayanasamy A, Chattopadhyay K, Manivel Raya M, Genesen K, Chinnasamay CN, Jeyadevan B. Low temperature magnetic properties and crystallisation behavior of finemet alloys. *J Appl Phys.* 2003;93:6182.
11. Gwizdała TM, Moneta M. Mössbauer distribution fitting by using global optimization approach. *Nucl Instrum Method Phys Res B.* 2012;B279:205.